REPORT DOCUMENTATION PAGE

Public reporting burden for this collection of information is estimated to average 1 hour per response, including the time for reviewing instructions, search ng existing data sources, gathering and maintaining the data needed, and completing and reviewing the collection of information. Send comments regarding this burden estimate or any other aspect of this collection of information, including suggestions for reducing this burden to Washington Headquarters Services, Directorate for Information Operations and Reports, 1215 Jefferson Davis Highway, Suite 1204, Arlington, VA 22202-4302, and to the Office of Management and Budget, Paperwork Reduction Project (0704-0188), Washington, DC 20503

1. AGENCY USE ONLY (Leave blank)	2. REPORT DATE February 1995	3. REPORT TYPE AND DATES COVERED Final, 30 Sep 93 - 29 Dec 94

4. TITLE AND SUBTITLE	5. FUNDING NUMBERS
Ceramics and Optics Laboratory Equipement Improvements	F49620-93-1-0518

6. AUTHOR(S)

Shankar M. Sastry and William E. Buhro

AFOSR-TR-96 97

0042

7. PERFORMING ORGANIZATION NAME(S) AND ADDRESS(ES)

Washington University
One Brookings Drive
St. Louis, MO 63130

9. SPONSORING/MONITORING AGENCY NAME(S) AND ADDRESS(ES)

Air Force Office of Scientific Research
AFOSR/NA
110 Duncan Ave, Suite B115
Bolling AFB DC 20332-8080

10. SPONSORING/MONITORING AGENCY REPORT NUMBER

11. SUPPLEMENTARY NOTES

12a. DISTRIBUTION/AVAILABILITY STATEMENT

Approved for public release, distribution is unlimited.

12b. DISTRIBUTION CODE

13. ABSTRACT (Maximum 200 words)

The X-ray diffractometer system purchased under the grant consists of an X-ray generator and associated equipment for determination of degree of crystallinity, crystallite size and lattice distortion in nano- and micro-crystalline metals and composites; identification of crystalline phases, precision measurment of lattice constants, and determination of phase transformation temperatures in metals, ceramics, and composites at 25-1400°C; determination of grain orientations, preferred orientation, and crystallographic texture by Laue back reflection pole figure mapping.

19970117 075

14. SUBJECT TERMS	15. NUMBER OF PAGES
Crystallography, metallurgy	18
	16. PRICE CODE

17. SECURITY CLASSIFICATION OF REPORT	18. SECURITY CLASSIFICATION OF THIS PAGE	19. SECURITY CLASSIFICATION OF ABSTRACT	20. LIMITATION OF ABSTRACT
UNCLASSIFIED	UNCLASSIFIED	UNCLASSIFIED	UNLIMITED

NSN 7540-01-280-5500

DTIC QUALITY INSPECTED 1

Standard Form 298 (Rev. 2-89)

HIGH TEMPERATURE X-RAY DIFFRACTOMETER FOR ADVANCED MATERIALS RESEARCH

Grant No. F49620-93-1-0518

FINAL TECHNICAL REPORT

Submitted to

by

Prof. Shankar M.L. Sastry (Principal Investigator)
and
Prof. William E. Buhro (Co-Principal Investigator)
Washington University
One Brookings Drive
St. Louis, MO 63130

February 25, 1995

TABLE OF CONTENTS

1. INTRODUCTION

X-ray Diffractometer (XRD) is a fundamental instrument for materials related research. To design the correct thermal treatments, to correlate the mechanical properties with the phases present, and to account for anisotropy in physical and mechanical properties of crystalline materials, XRD measurements are essential. Our group at Washington University have active research programs in the synthesis, processing, and characterization of advanced high performance structural and functional materials which require state-of-the-art X-ray diffraction measurements. This report summarizes the X-ray diffraction equipment that was purchased under the AFOSR Grant No. F49620-93-1-0518, and the research projects in which the X-ray diffraction equipment has been used thus far.

2. DESCRIPTION OF THE HIGH TEMPERATURE X-RAY DIFFRACTOMETER:

The X-ray Diffractometer system purchased under the grant consists of an x-ray generator and associated equipment for determination of degree of crystallinity, crystallite size and lattice distortion in nano-and micro-crystalline metals and composites; identification of crystalline phases, precision measurement of lattice constants, and determination of phase transformation temperatures in metals, ceramics, and composites at 25-1400°C; determination of grain orientations, preferred orientation, and crystallographic texture by Laue back reflection pole figure mapping. The major components purchased are:

1. Model D/Max-3BX Horizontal X-ray Diffractometer
2) Diffracted Beam Monochromator
3) Pole Figure Attachment
4) High Temperature Furnace Attachment
5) IBM PS Value Point Computer System
6) Qualitative/Quantitative Software
7) JCPDS Data Base.

2.1 Horizonal X-ray Powder Diffractometer:

The diffractometer shown in Figure 1, consists of a 3.0 kW X-ray generator for single X-ray tube to operate at 60 kV, 80 mA with a stability of + 0.01%, a horizontal wide angle angle goniometer with dual axis driver for independent or coupled theta/2theta drive and step scan, a 2.0 kW Cu target X-ray diffraction tube with normal focus of 1 x 10 mm, a scintillation counter assembly, power supply, a D/Max-B control driver unit, a goniometer control board, and 2kVA electrostatically shielded isolation step down transformer with 200 x 100 V input and 200/100V output.

2.1.1 X-ray Generator:

The x-ray generator (model no. TR-58 DXG3 3kW; catalog No. 4057A2) shown in Figure 2 is designed to generate stable high voltage through a full-wave rectified circuit. The generator can be operated in both manual and automatic modes. The automatic operation is available using external control feature in combination with Rigaku D/max-B system. The control features include the power on/off, X-ray on/off, and tube voltage and current settings.
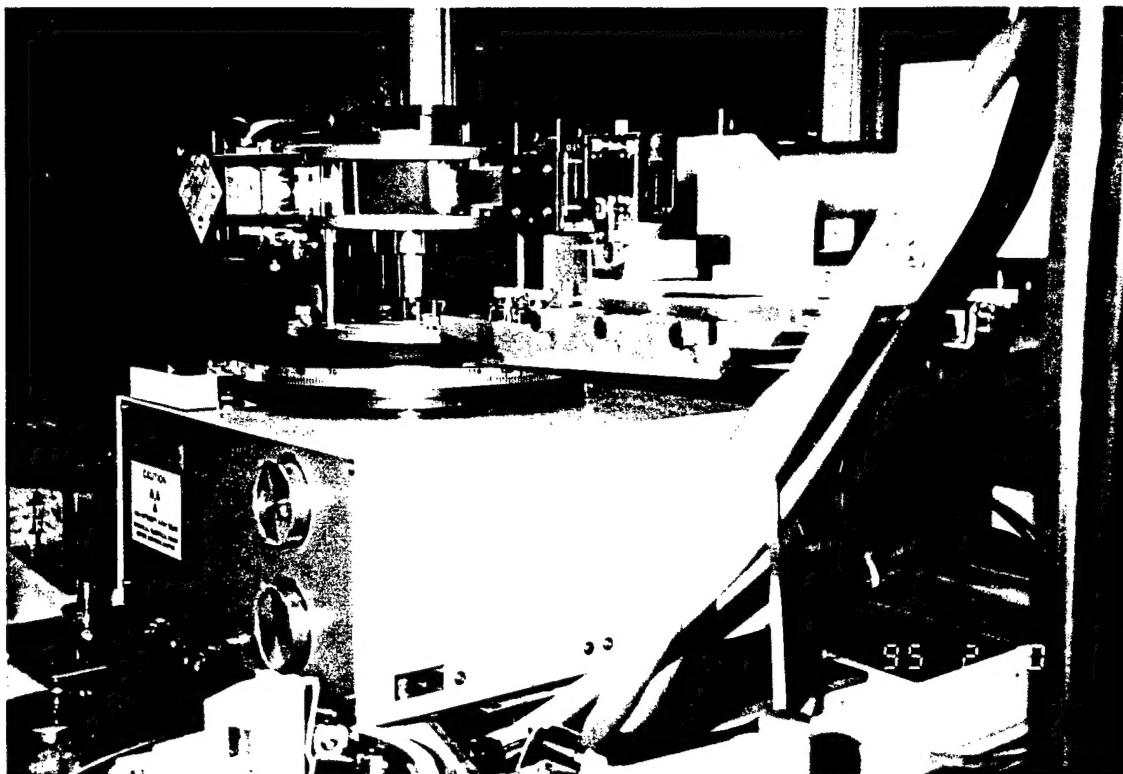
Figure 1. Photograph of Rigaku D.Max-3B Horizontal X-ray Diffractometer
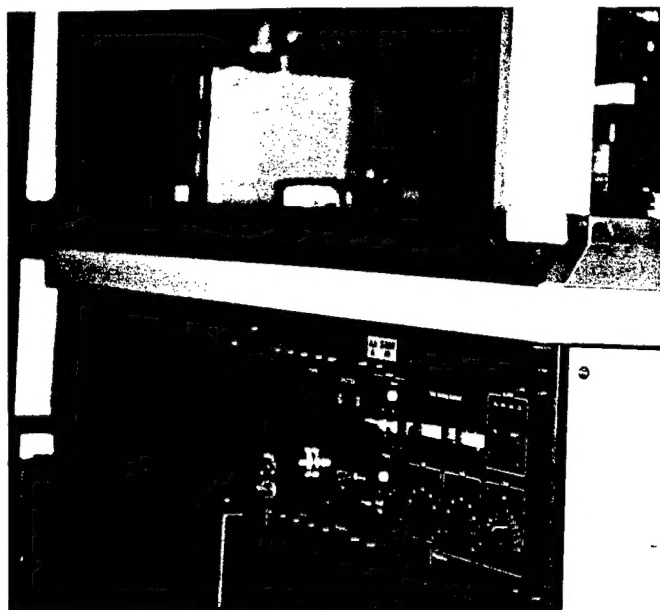

Figure 2. Photograph of X-ray Generator

2.1.2 Goniometer:

The goniometer (shown in Figure 3) is designed to satisfy the focusing condition geometrically, shown in Figure 4. The focusing circle is a circle on the plane which involves the center of the sample and at the right angle with the axis of rotation of the goniometer, and the circle involves the axis I of the focus of the target, the axis II of the goniometer, and the axis III of the receiving slit. In order to satisfy the focusing condition, it is required to satisfy the following conditions: (1) The axis I of the focus, the rotating axis II of the goniometer, and the axis III of the receiving slit must be on the parallel line, (2) the projection falling upon the surface of the sample involving the plane of the focusing circle is a line, which is tangent to the focusing circle, (3) the center of the surface of sample must be on the rotating axis of the goniometer, (4) the axis I of the focus and the axis II of the receiving slit must be at equal distances from the center of the surface of the sample, and (5) the respective centers of the focus, the surface of the sample and the receiving slit must be on the plane at the vertical angle toward the rotating axis of the goniometer. The design and structure of each section of the goniometer are made to satisfy the above conditions either automatically or by settings.

The goniometer is equipped with a specimen rotation attachment designed for the reflection and transmission x-Ray diffraction. The attachment is aimed to reduce the undesirable effects associated with large crystals grains of specimens.

2.1.3 X-Ray Tube and Shield Assembly:

A 2.0kW Cu target X-ray tube and high voltage cable are contained in a tube housing shown in Figure 5. There is an x-ray window each at the right and left sides and the windows are used to in common for line and point focus. An electromagnetic shutter is attached at each side. The housing head has two holes one for the inlet and the other for outlet for target water-cooling pipe.

2..1.4 Scintillation Counter:

The scintillation counter assembly consists of a NaI scintillator of 29 mm outside diameter and an effective diameter of 18 mm, a photomultiplier with a maximum anode voltage of 1500 V D.C and a preamplifier. The application of high voltage to the photo-multiplier, that of voltage to the preamplifier and taking-out of output signals are accomplished through the 5-pin connector and the 3-cord cable.

2.2 Monochromator:

The x-ray monochromator (Figure 6) for the X-ray diffractometer counter is attached to the counter arm of the goniometer to monochromatize x-ray diffraction lines of a sample. The diffracted x-rays monochromatized by a a [0002] graphite curved single crystal are transmitted into the counter.
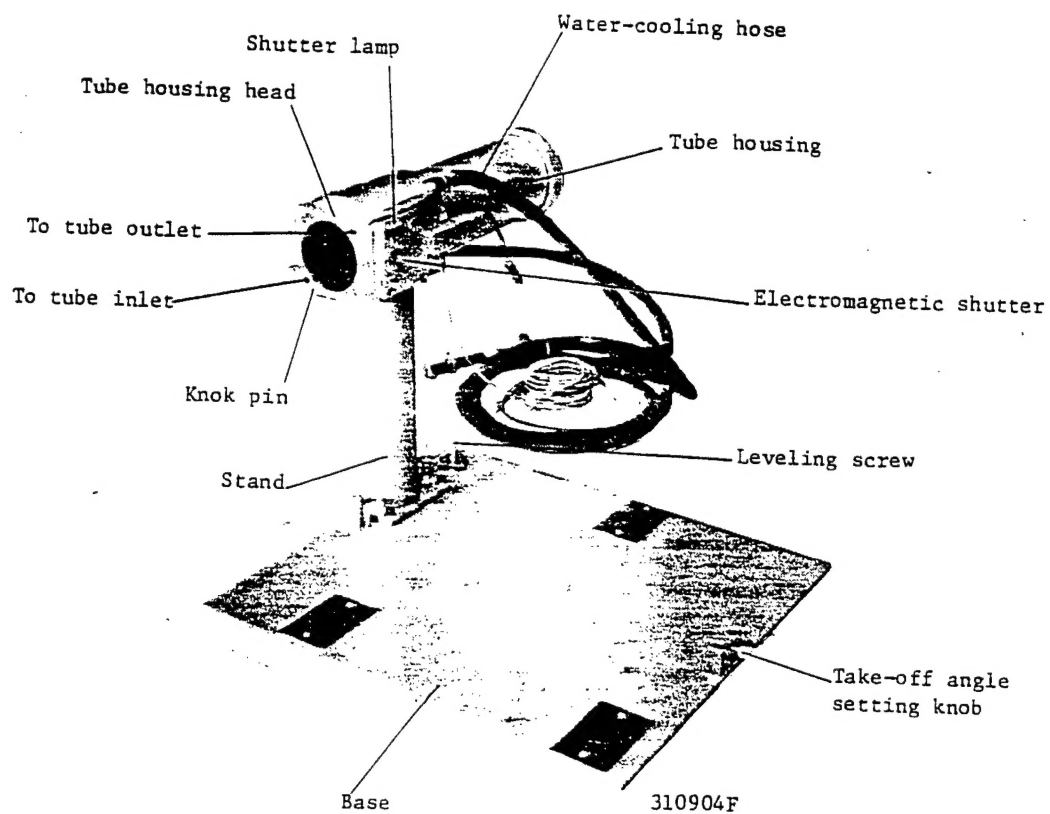
Figure 5. X-ray Tube and Shield Housing

Labels: Shutter lamp, Water-cooling hose, Tube housing head, Tube housing, To tube outlet, To tube inlet, Electromagnetic shutter, Knok pin, Leveling screw, Stand, Take-off angle setting knob, Base, 310904F
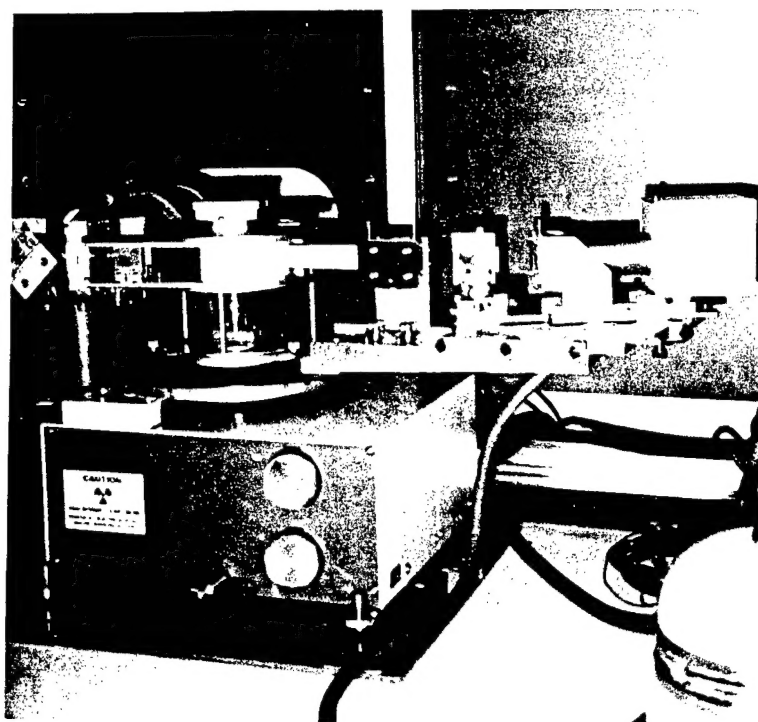

Figure 6. X-ray Monochromator

2.3 Pole Figure Diffractometer Attachment:

A semi-automatic pole figure attachment to be used in conjunction with the diffractometer for analyzing the texture of plate specimens is shown in Figure 7. This attachment is used for expressing the preferred orientation of texture on a stereographic projection parallel to the specimen surface as a pole density. This can be attained by rotating the specimens round two axes A and B perpendicular to each other. In order to obtain information from the entire specimen, the specimen has to be set in reciprocating motion (gamma-oscillation). The rotation angle ranges required around both axes A and B are 0-90° and 0-360° respectively.

Figure 8 shows the principle of the pole figure attachment. If a specimen has preferred orientation (aggregate texture), the intensity in terms of counts after conducting absorption correction of this specimen will vary with the movement of the specimen (rotations around 2 axes. These intensity variations are expressed as a polar density distributions on the polar net for stereographic projection. The movement of the specimen is performed through rotations around its two axes A and B which intersect each other at right angles. The rotation around the axis A is called alpha-rotation while the rotation around the axis B (normal to the specimen plane) is called beta-rotation. Beta-rotation is first carried out at a certain alpha angle by continuous or stepwise feed, then stepwise feed of the alpha angle is done, followed by beta-rotation again.

2.4 High Temperature X-Ray Diffractomter Attachment:

High temperature X-ray diffractometer attachment, Cat. No. 2311B1 (shown in Figure 9) is designed to maintain a specimen at high temperature and record its diffracted X-rays automatically under respective high temperature either in vacuum, inert gas, or in air. When the attachment is used in combination with the Rigaku program temperature controller, the specimen temperature can be kept constant or can be controlled precisely.

The furnace, made from the alumina frame work and the platinum heater 0.6 mm diameter, (Figure 10) has very small heat capacity. Heater wire of the furnace is routed parallel to the X-ray path to obtain maximum X-ray intensity. Two pairs of thermocouples are used; one, a Pt, Pt- 13% Rh, 0.2 mm diameter is for temperature measurement and another 0. 3mm dia of Pt, Pt- 13% Rh,is used for temperature control. The attachment can be used upto 1500°C in vacuum, or 1400°C in inert gas or air.

2.5 Control/Data Processing Unit:

The Rigaku D/max system and an IBM compatible personal computer are combined for automated measurement as well as for various analyses of measurement data. The system carries out efficient controls by taking full advantage of the computer performance. The personal computer and the control driver are connected to each other with a serial line (RS232C). The control driver directly controls each section of the diffractometer based on control commands given by the personal computer.

2.6 Qualitative and Quantitative Software Package:

The software package is of two types: the standard part and the application part. The standard part comprises program groups for measurement of powder diffraction patterns by the use of different types of goniometers, general processing of the resulting measurement data (file editing, plotter display, peak detection, etc.,), and the system diagnosis, adjusting, and auxiliary operations. The application part is composed of application program groups related to a variety of application measurements and data analyses.
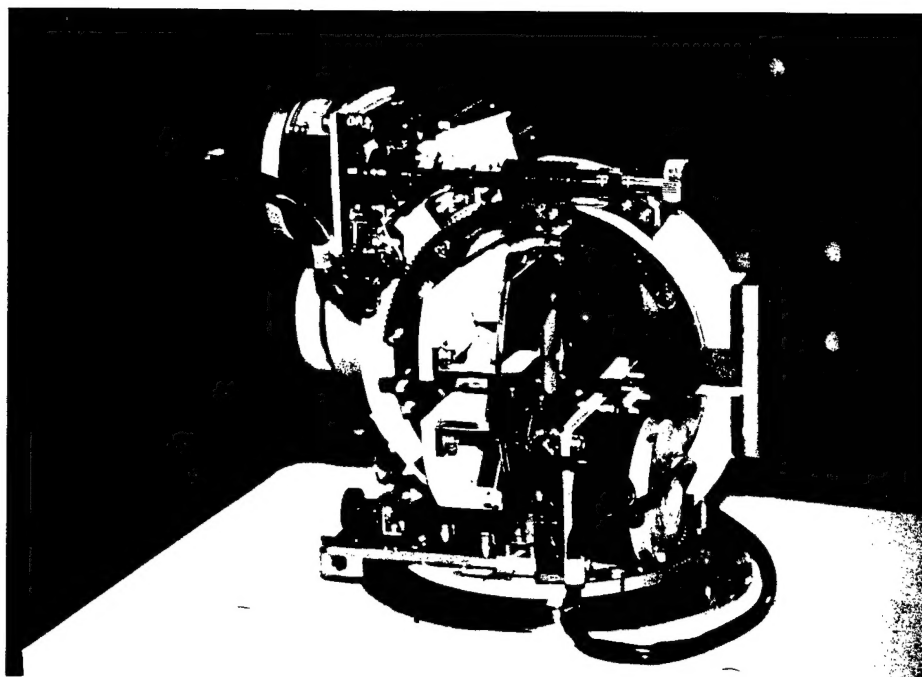
Figure 7. Pole Figure Diffractometer Attachment:

(a) Fundamental Principle of Transmission Method

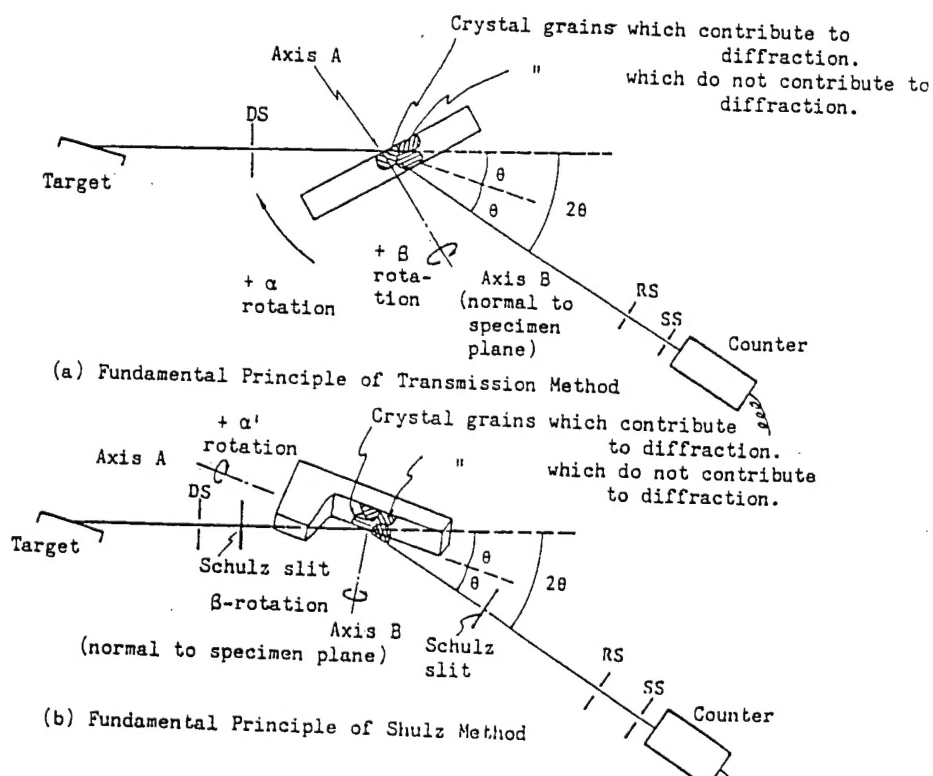(b) Fundamental Principle of Shulz Method

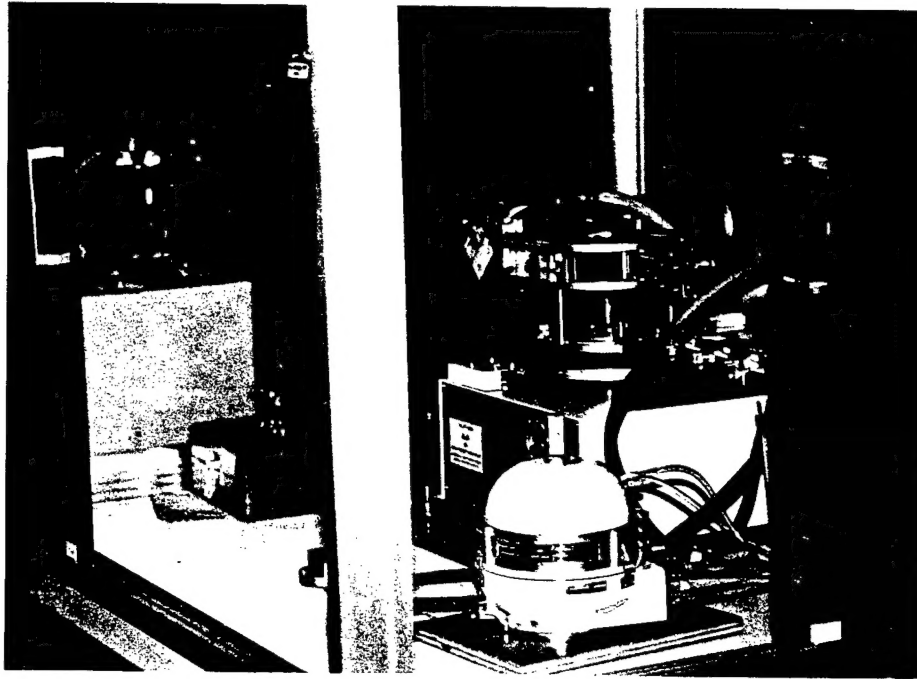**Figure 8. Schematic Illustrating the Basic Principles of Pole Figure Attachment**

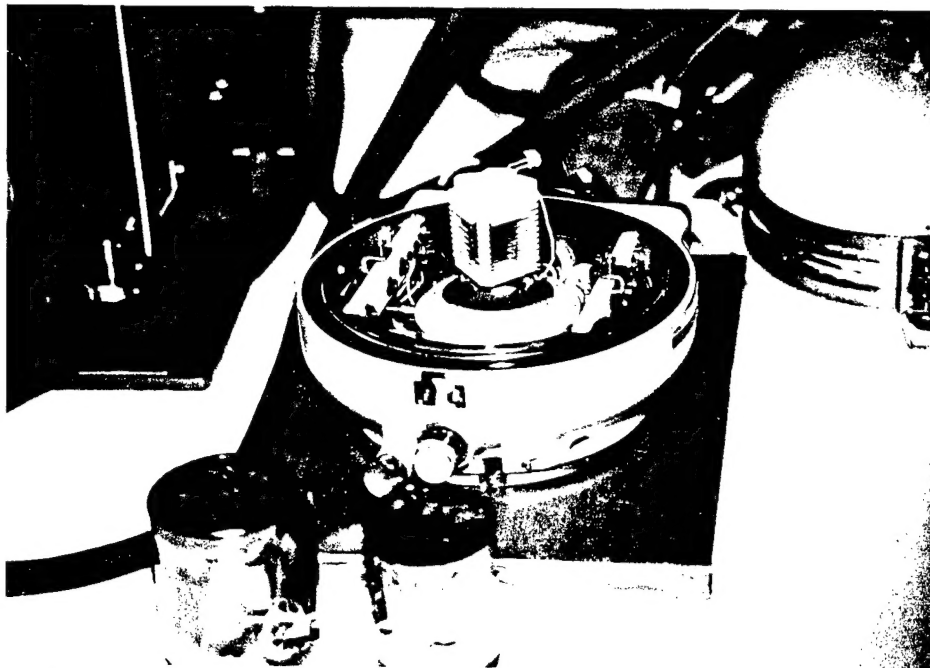Figure 9. High Temperature X-ray Diffractometer Attachment:

Figure 10. Close-up of the High Temperature X-ray Diffractometer Attachment showing the details of the furnace assembly.

3.RESEARCH PROJECTS CONDUCTED USING THE X-RAY DIFFRACTOMETER:

3.1 Undercooling and Supersaturation of Alloying Elements in Rapidly Solidified Al-8.5% Fe- 1.2 % V- 1.7% Si Alloy.

X-Ray diffraction analysis was performed to study the dependence of supersaturation of alloying elements and metastable phase formation on the extent of undercooling. An alloy of nominal composition Al-8.5%Fe-1.2%V-1.7%Si was produced by inert gas atomization (IGA) and atomized melt deposition (AMD) processes. The alloy powder was sieved to obtain powders of various size fractions. The size fraction less than 30 μm and fraction of 180μm < d < 250 μm were annealed in a vacuum of 10^{-6} torr at 430 ° C for 24 hours. The atomized melt deposited alloy was tested in the as deposited condition and after thermo-mechanical processing. The alloys were thermomechanically processed by hot-isostatically pressing at 410°C and 203 MPa for 4 h and extruding into 6 mm diameter rods at 400°C with an extrusion ratio of 16:1. X-ray diffraction analyses were performed on gas atomized powders in as processed and annealed conditions and on AMD deposits in as deposited and extruded conditions to identify the phases produced under different rapid solidification conditions.

Figures 11(a)-(c) show the X-ray diffraction results for planar flow cast (PFC) alloy sheet and the IGA alloy in as processed and annealed conditions. The diffraction pattern indicates the differences in the phases present for the powder alloy for different powder sizes in as processed and annealed conditions. The X-ray diffraction pattern for the AMD alloys are shown in Figures 12 (a)-(b).

During rapid solidification processing, the alloy is cooled through a non-equilibrium phase region leading to the formation of metastable phases and supersaturation of solute elements in the solid solution. When the rapidly solidified alloy is reheated as in the case of DSC experiment, the phases allowed by non-equilibrium kinetics will undergo solid state transformation and the supersaturated alloying elements in the matrix precipitate out to form new metastable phases. The $Al_{12}(Fe,V)_3$ Si phase with BCC crystal structure, precipitates out from the supersaturated matrix when the Al-8.5%Fe-1.2%V-1.7%Si alloy is heated to about 425 ° C. Figure 11(a) shows the presence of precipitated $Al_{12}(Fe,V)_3$ Si phase in the case of PFC alloy sheet which was hot iso-statically pressed and extruded at 420 °C using communited planar flow cast ribbons . In the case of finer as processed powder alloy of size less than 30 μm where supersaturation levels are high, the presence of $Al_{12}(Fe,V)_3$ Si phase is less evident as seen in Figure 11(b). But on annealing at 430 ° C , the $Al_{12}(Fe,V)_3$ Si phase precipitates out and hence the presence of $Al_{12}(Fe,V)_3$ Si phase peaks increase as seen in Figure 11(b). In as processed coarser powder alloy of size greater than 180 μm , supersaturation of alloying elements is low due to lower level of undercooling achieved during processing. As seen from the Figure 11(c), new phase formation is not seen in the X-ray diffraction pattern after annealing except for the peaks of $Al_{12}(Fe,V)_3$ Si phases which coarsen and are already present before annealing. Similarly in the case of AMD alloy-, where the supersaturation levels were higher, peaks of precipitated $Al_{12}(Fe,V)_3$ Si phase are more evident than in the case of AMD alloy-2 where the supersaturation levels were not high. The results clearly demonstrate that the supersaturation of alloying elements is directly dependent on the undercooling experienced during solidification of the alloy.
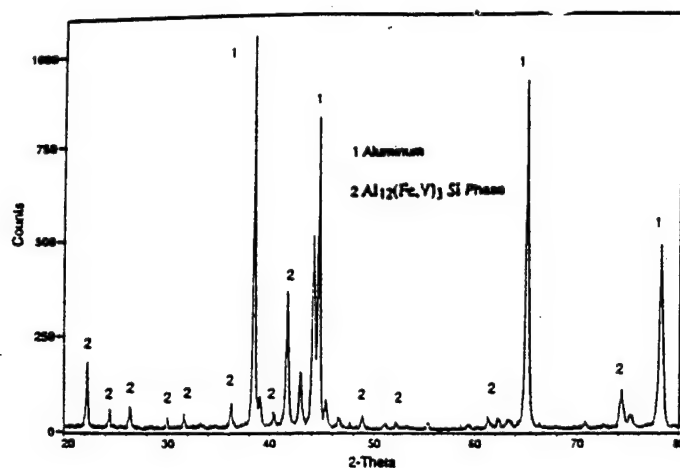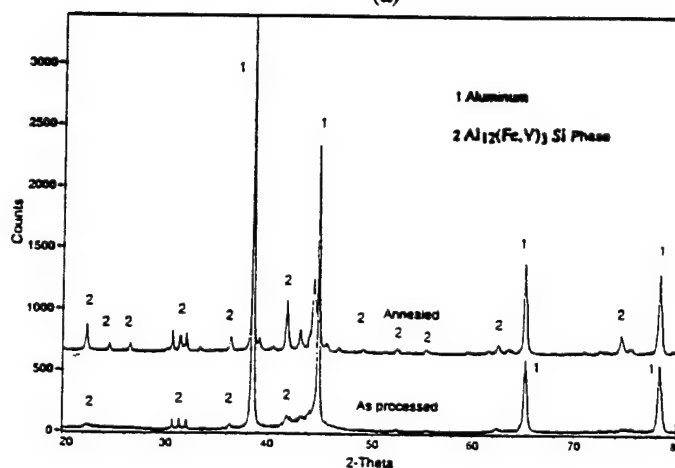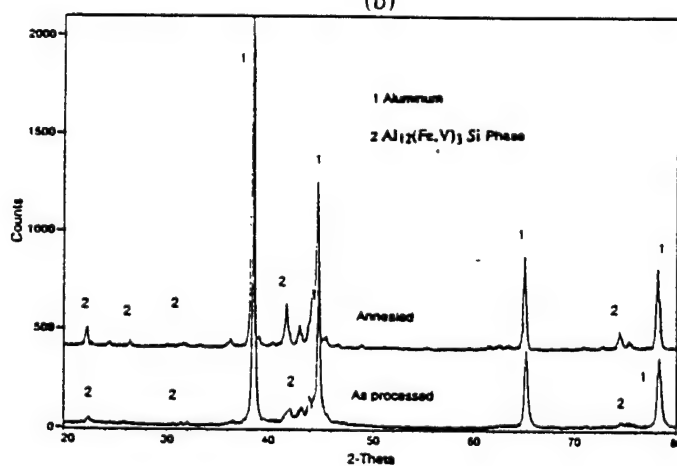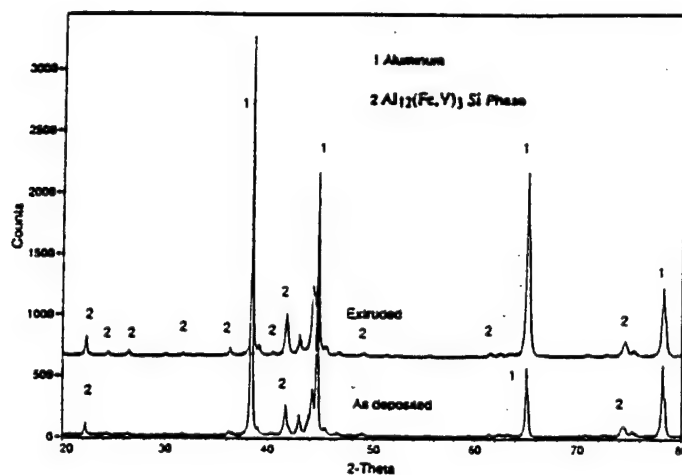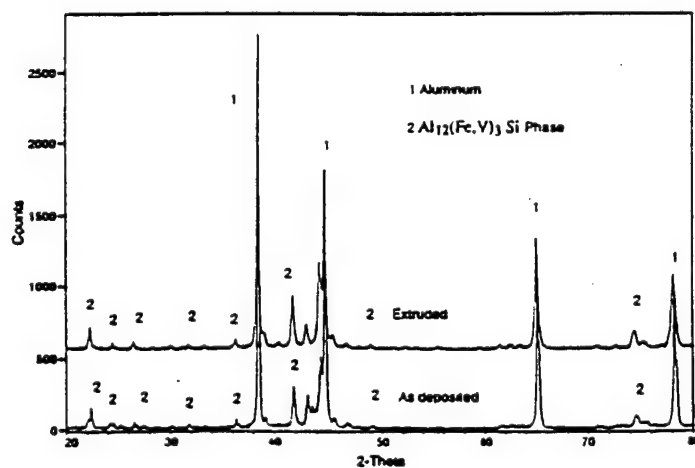
Figure 11. X-ray diffraction pattern for Al-8.5%Fe-1.2%V-1.7%Si alloy produced by (a) Planar Flow Casting, (b) Inert Gas Atomization of powder size < 30 μm and (c) Inert Gas Atomization of powder size fraction of 180μm < d < 250 μm.

(a)

(b)

Figure 12. X-ray diffraction pattern for Al-8.5%Fe-1.2%V-1.7%Si alloy produced by Atomized Melt Deposition process. (a) AMD alloy-1 and (b) AMD alloy-2.

3.2 Characterization of Nanocrystalline Molybdenum Disilicide Produced by Sonochemical Synthesis:

Sonochemical co-reduction of $MoCl_5$ and $SiCl_4$ with NaK alloy in a hexane dispersion using 600 W, 20 kHz irradiation, followed by annealing at 900°C produces nanocrystalline $MoSi_2$ powders with 90% yield. X-ray diffraction patterns of the powders revealed both the alpha (low-temperature) and beta (high-temperature) phases of $MoSi2$ be present, and indicated average crystallite coherence lengths in the range of 16-31 nm, depending on annealing time (Figure 13a). X-ray diffraction analysis of consolidated powder sample confirmed the material to be alpha $MoSi_2$ having an average crystallite coherence length of 31 nm (Figure 13b).

3.3 Characterization of Nanocrystalline Ti and TiB_2 Produced by Gas Phase Combustion Synthesis and Solution Phase Synthesis:

Figure 14 shows a typical X-ray diffraction spectrum of nanocrystalline Ti produced by gas phase combustion synthesis employing the exothermic reaction:

$$TiCl_4 + 4\,Na \text{ -----------------> } Ti + 4\,NaCl$$
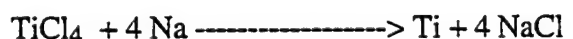
One of the objectives of the above synthesis method was to produce an in-situ salt coating on nanocrystalline Ti to prevent the oxidation of nanocrystalline Ti. To determine the effectiveness of NaCl coating as an oxidation barrier coating, the powder produced by the above reaction was stored in air for 3 days and analyzed in air. As seen in Figure 14, all peaks accurately index to either NaCl or Ti. The presence of Ti suggests that the salt coating is acting to inhibit oxidation of Ti. The corresponding crystallite sizes as determined by the XRD pattern are 30 nm for Ti and 70 nm for NaCl.

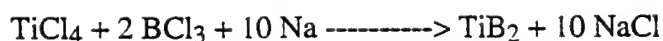Nanocrystalline TiB_2 particles were produced using the reaction

$$TiCl_4 + 2\,BCl_3 + 10\,Na \text{ ----------> } TiB_2 + 10\,NaCl$$

Figure 15 is an XRD spectrum of a typical powder produced in an $Na/TiCl_4/BCl_3/Ar$ flame where the NaCl has been removed by water wash and centrifuge. The peaks in the spectra index to TiB_2 and show a nominal particle size of 6 nm. The large amorphous background suggests that the particles are either not fully crystalline or that much finer particles exist.

3.4 Solution-Phase Synthesis of TiAl and NiAl :

Solution-phase processing is an extremely promising new strategy for producing nanometer-scale particles of metals, intermetallics and ceramics. In this method solution-phase chemical reactions are conducted at low temperatures (< 200 °C) in solution to afford solid precursors to nanocrystalline particles. The solid precursors obtained from such solution-phase reactions are extremely reactive powders comprising very small primary particles (sizes ca. 1 - 5 nm). These reactive powders are subsequently annealed in the solid state at temperatures of ca. 500 - 1000 °C, resulting in the nucleation and growth of 10 - 100 nm crystallites. We have now obtained nanocrystallites of TiB_2, ZrB_2, TiC, TiN, $MoSi_2$, Ni_3Al, NiAl, TiAl, and $TiAl_3$ by solution-phase processing, and are optimizing their production. Significantly, the sizes and morphologies of the nanocrystallites depend on the conditions employed.
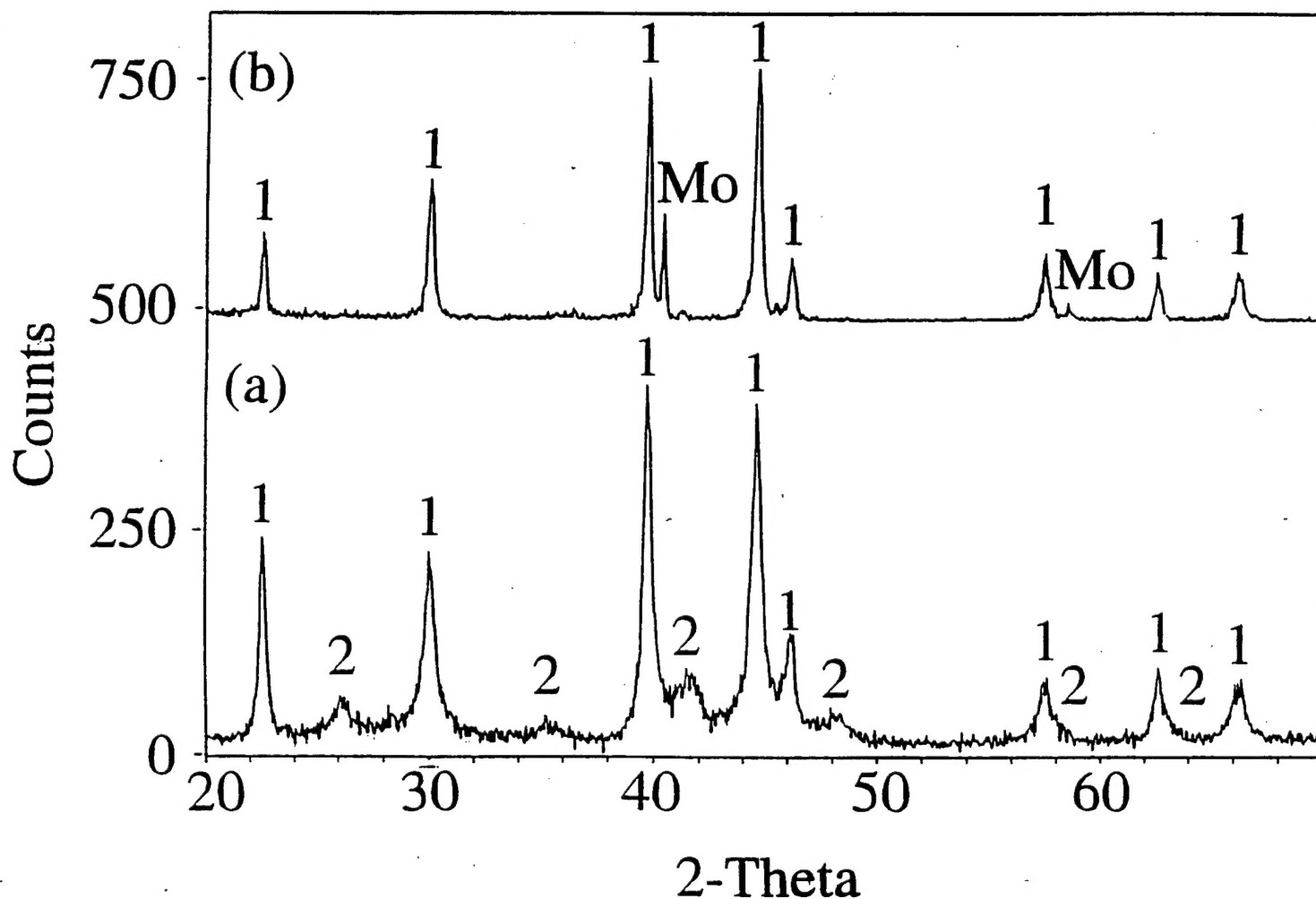
Figure 13. (a) XRD pattern of nanocrystalline $MoSi_2$ powder annealed at 900°C for 5 min. The phases present are alpha-$MoSi_2$(1, low-temp phase) and beta-$MoSi_2$(2, high-temp phase). The crystallite coherence length calculated by the Scherrer equation using reflections from alpha-$MoSi_2$ was 16 nm. (b) XRD pattern of the hot pressed $MoSi_2$ compact; the crystallite coherence length was 31 nm. The minor reflections assigned to Mo metal are the result of extrinsic surface contamination of the compact by partial degradation of the TZM punch.
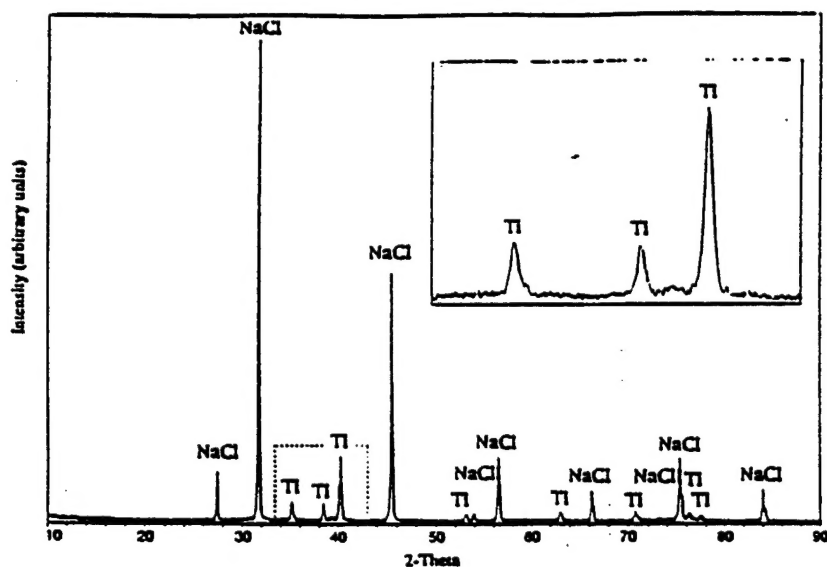
Figure 14. Typical X-ray diffraction pattern for an as-prepared Ti/NaCl powder generated from an Na/TiCl$_4$/Ar flame
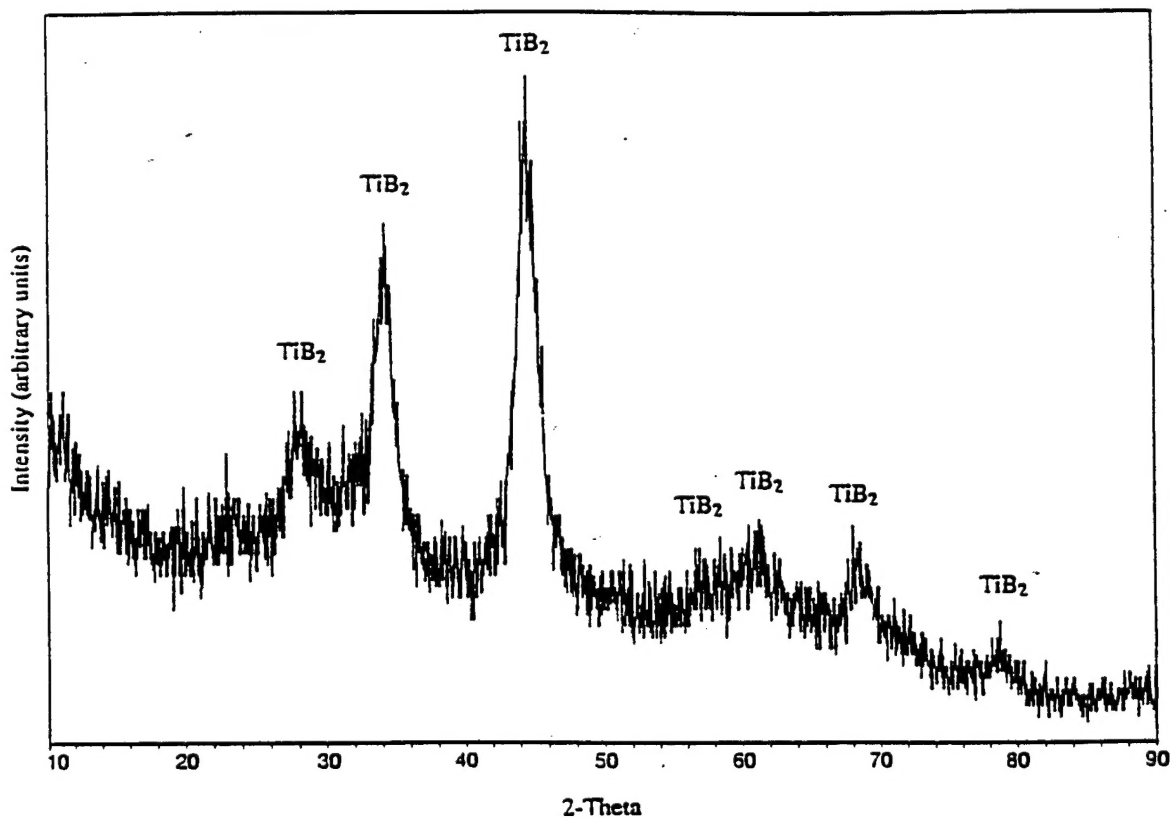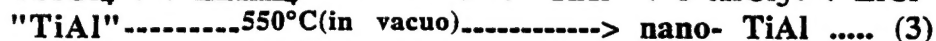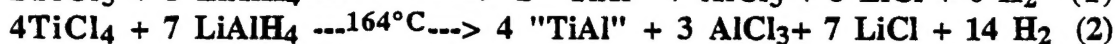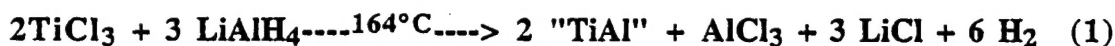

Figure 15. Typical X-ray diffraction pattern for water-washed TiB$_2$sample generated from a Na/TiCl$_4$/BCl$_3$/Ar flame.

The chemical reactions employed in solution-phase processing to produce TiAl and NiAl are shown below:

$$2TiCl_3 + 3\ LiAlH_4 \xrightarrow{\quad 164°C \quad} 2\ \text{"TiAl"} + AlCl_3 + 3\ LiCl + 6\ H_2 \quad (1)$$
$$4TiCl_4 + 7\ LiAlH_4 \xrightarrow{\quad 164°C \quad} 4\ \text{"TiAl"} + 3\ AlCl_3 + 7\ LiCl + 14\ H_2 \quad (2)$$
$$\text{"TiAl"} \xrightarrow{\quad 550°C(\text{in vacuo}) \quad} \text{nano- TiAl} \quad ..... \quad (3)$$
$$4\ NiCl_2 + 5\ LiAlH_4 \xrightarrow{\qquad} 4\ NiAl + AlCl_3 + 5\ LiCl + 10\ H_2 \quad (4)$$

All the chemical reactions listed above are straightforward, convenient, and use readily available starting materials. Our procedures could easily be conducted on tens to hundreds of kilogram scales by the chemical industry, making solution-phase processing industrially viable. In addition to the advantages of simplicity and scale, solution- phase processing is considerably more versatile than some of the other methods. The sonochemical coreduction method, one variant of solution-phase processing under development here for the preparation of $MoSi_2$ (AFOSR Grant No.F 49620-93-0131), allows for the simultaneous, uniform reduction of mixtures of metal (metalloid) salts, affording homogenous intermetallic nanocrystallites.

X-ray powder diffraction patterns of the nanocrystalline TiAl and NiAl particles produced by SPS are shown in Figures 16 and 17.
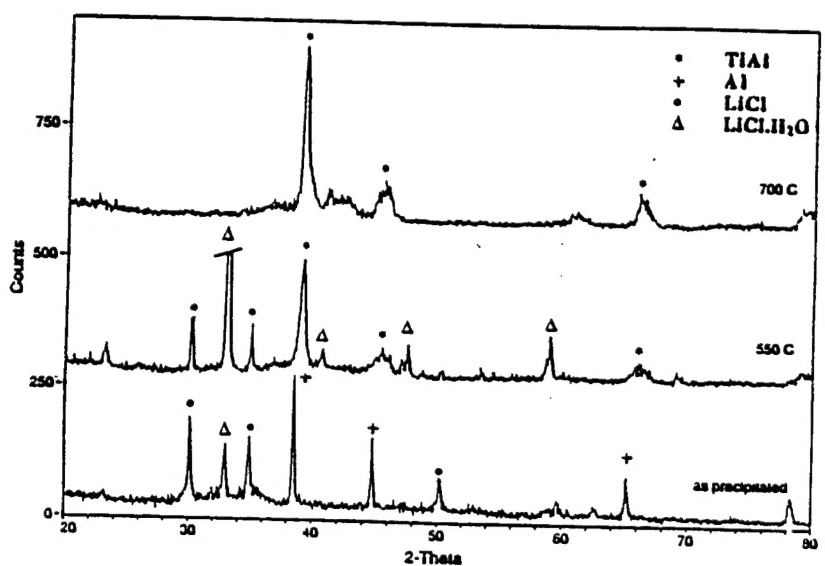
Figure 16. X-ray Diffraction Spectra of Nanocrystalline TiAl Produced by Solution-Phase Synthesis.
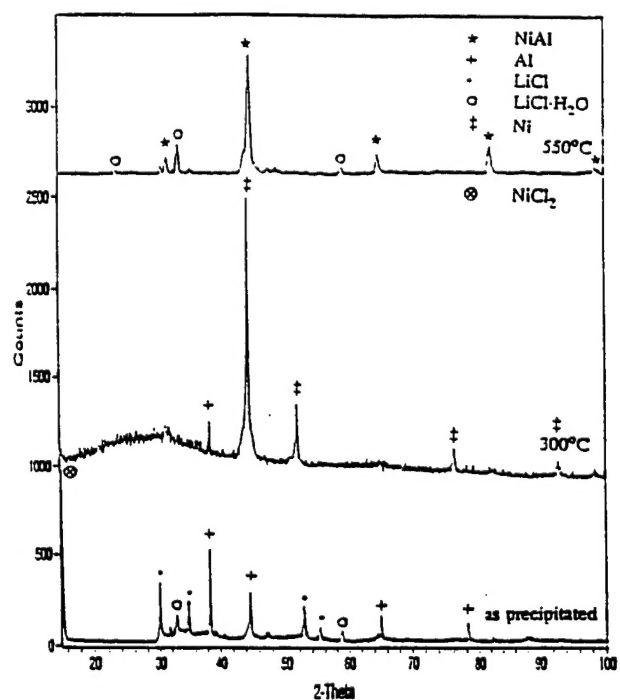

Figure 17. X-ray Diffraction Spectra of Nanocrystalline NiAl Produced by Solution-Phase Synthesis.